



Microstructure Contributions to Vibrational Damping and Identification of Damage Mechanisms in Arundo Donax L: Reed Cane for Woodwind Instruments

Journal:	<i>2016 MRS Fall Meeting</i>
Manuscript ID	MRSF16-2553795.R2
Manuscript Type:	Symposium TC3
Date Submitted by the Author:	13-Feb-2017
Complete List of Authors:	Kemp, Connor; McGill University Scavone, Gary; McGill University
Keywords:	biomaterial, internal friction, microstructure

Microstructure Contributions to Vibrational Damping and Identification of Damage Mechanisms in *Arundo Donax L*: Reed Cane for Woodwind Instruments

Connor Kemp¹ and Gary Scavone¹

¹Computational Acoustic Modeling Laboratory, McGill University, 555 Sherbrooke Street West, Montreal, QC, Canada.

ABSTRACT

Natural cane reeds (Latin name *Arundo Donax L* and here termed ADL) have been used on woodwind instruments for centuries with little change. The reed acts as a mechanical valve controlling the energy input into the musical instrument and it is the musician's first option for altering the instrument's sound and response characteristics. Despite this, their consistency, variable performance, durability and sensitivity to ambient conditions make it difficult for the musician to find and maintain a reed that responds to their liking. Thus it is desirable to examine the material, microstructural and anatomical properties of the reed and their contributions to vibrational performance with input from mechanical engineers, materials scientists and musicians.

The current study is part of an on-going research project, and this paper presents preliminary results. In the present work raw samples of ADL obtained from a manufacturer in pre-cut form are sectioned into longitudinal and transverse specimens for mechanical characterization. Prior to testing, samples are conditioned using an incubation system to 37 degrees Celsius and 90% relative humidity, mimicking in-use conditions of the reed. Initial microstructure analysis of each specimen is completed using optical microscopy to quantify fiber spatial arrangement, size and the existence of micro-cracks along the fiber-matrix interface. X-ray diffraction is also used to quantify the fraction of crystalline cellulose present in each sample. Specimens are then excited over a specific frequency range similar to that of in-use reeds using pressure waves in a non-contact setup. Values of internal friction are obtained as logarithmic decrement values for frequency-dependent decay. One set of specimens is then subjected to cyclic mechanical loading at low frequency (< 1 Hz) and stresses up to 15MPa. The other set is maintained at the given environmental conditions using the incubator and aged through temperature and humidity cycling. Comparisons of post-testing microstructure damage and internal friction measurements are then completed to delineate specific degradation mechanisms due to mechanical/fatigue deterioration and moisture cycling. Internal friction is found to be dependent on both frequency, moisture and cyclic loading. Furthermore, the existence of microstructural cracks contributes to increasing decrement values at high frequencies in both fatigued and moisture cycled samples. Statistically significant correlations are discovered between logarithmic decrement and vascular bundle orientation at 700 Hz and logarithmic decrement and parenchyma cell diameter at 1000 Hz. Reductions in internal friction below 400 Hz indicate a decreasing loss modulus (E'') with increased moisture cycles, although this trend will be tested against a larger sample set in further work.

INTRODUCTION

The reed is a small piece of cane (*Arundo Donax L.*, here termed ADL) that is used on many woodwind instruments as the primary vibrating element. This element controls the volume flow of air into the air column and is critically important to the sound produced by the instrument. Reeds are often found to be highly variable, both in terms of static stiffness and produced sound. Despite this, little research has been conducted on the material properties and microstructural contributions to this variability. Furthermore, little is known about the reed material ADL in terms of its elastic, plastic, dynamic, degradation and damping properties. An example of an ADL microstructure is provided in Figure 1. This work presents a proposed methodological framework to study structural changes in reed material (ADL) when exposed to in-use conditions and the framework is demonstrated using four compression samples.

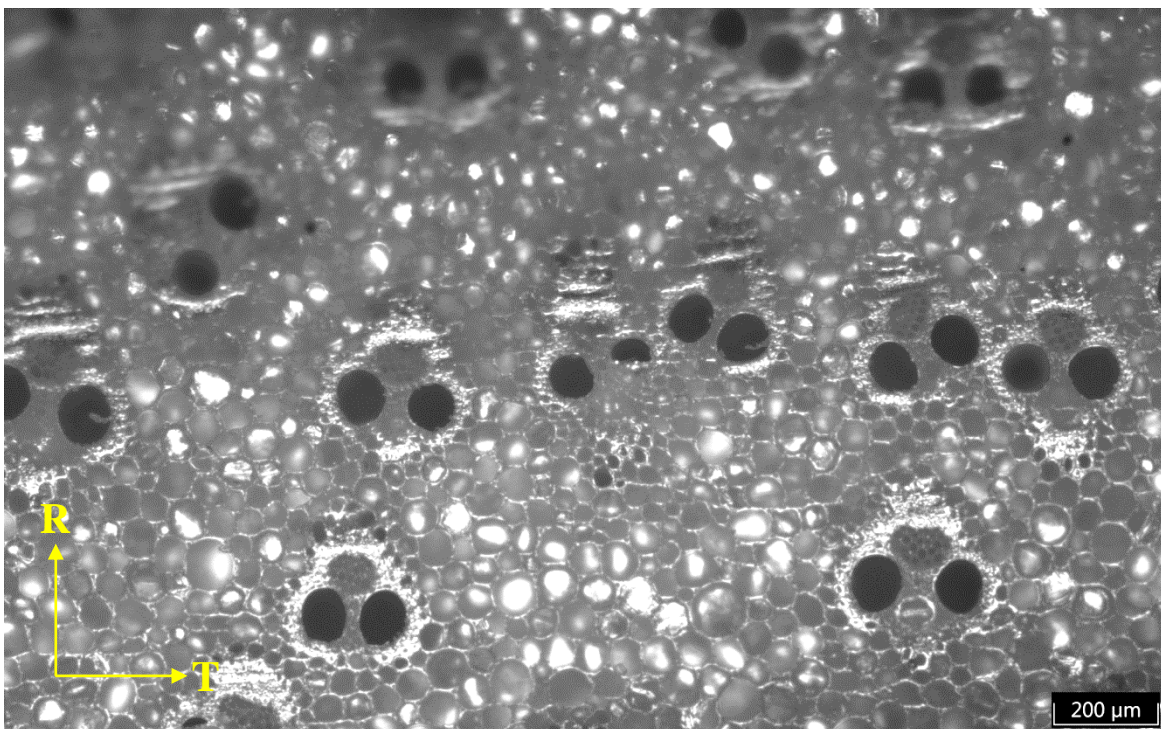


Figure 1: ADL microstructure as a cross-section through the stem. This orientation shows fibers and vascular bundles aligned in the longitudinal direction.

Similarities can be drawn to bamboo in terms of the structures present in this material, primarily the vascular bundles, fiber cap and parenchyma matrix. Like bamboo and most wood materials, ADL can be considered as elastically orthotropic with fibers aligned in the longitudinal direction of the stem. For this material the three important directions are axial/longitudinal, radial (*R* in Figure 1) and tangential/transverse (*T* in Figure 1). Stiffness in ADL is provided by the fibers and fiber caps within the porous matrix of parenchyma. Fibers and fiber caps can be observed as the light sections surrounding the large, open vessels (lumen) of Figure 1. Reeds are manufactured with their cross-section aligned with the longitudinal direction of the stem. Despite this and sophisticated machining techniques, natural variations in stem size and straightness can cause misalignment with the fibers resulting in less predictable stiffness. The reed tip is also $\sim 100\mu\text{m}$ in thickness which contributes to this variability as there is no separation of length

scales. This tip is also exposed to large strains, likely large enough to induce permanent deformation [1].

To complicate matters further it is also well known that reed properties can change during their useable lifespan. As reeds are played in a fully humidified state (and stored either in a dry or semi-humidified state), changes in elastic and damping properties are not well understood. Also the roles that moisture degradation and mechanical degradation (here, cyclic fatigue loading from playing) play in contributing to these changing properties have not been examined for ADL. The present study is part of ongoing research and presents preliminary observations of changes in the dynamic behavior (damping properties) of ADL due to cyclic mechanical loading and moisture cycling. Both of these cases are chosen to mimic the in-use conditions that a reed is routinely exposed to, namely induced mechanical oscillations of the reed tip and humidity changes between playing conditions and storage conditions.

In the context of materials science, this study considers damping properties via internal friction measurements of the logarithmic decrement of free vibration. This method is chosen due to the constraints of sample geometry and size, and its elegance of simplicity. The logarithmic decrement has been used frequently as a measurement of internal friction and can be measured using resonant bar techniques, the torsion pendulum, or high frequency driven oscillation, to name just a few. Here the resonant bar technique (similar to [2]) is used and is outlined in detail in a subsequent section. X-ray diffraction is also used to observe differences in the crystalline fraction of cellulose between each. Measured differences in internal friction are compared with XRD measurements and microstructural parameters in an effort to correlate material properties with sample performance. Given the limited number of samples tested to-date (4), only trends in the data are discussed as opposed to absolute values of internal friction, microstructural features and crystallinity.

EXPERIMENT

The present study consists of two main components including cyclic mechanical loading and relative humidity (RH) cycling. Measurements of internal friction are taken before, during and after each step of the experimental procedure. There were four material specimens in total, including two of each material orientation as shown in Figure 2 (two samples transverse to the long-axis of the stem and two samples parallel to the long axis). For reference, the micrograph provided in Figure 1 is a cross-section of the stem wall microstructure (inner to outer diameter).

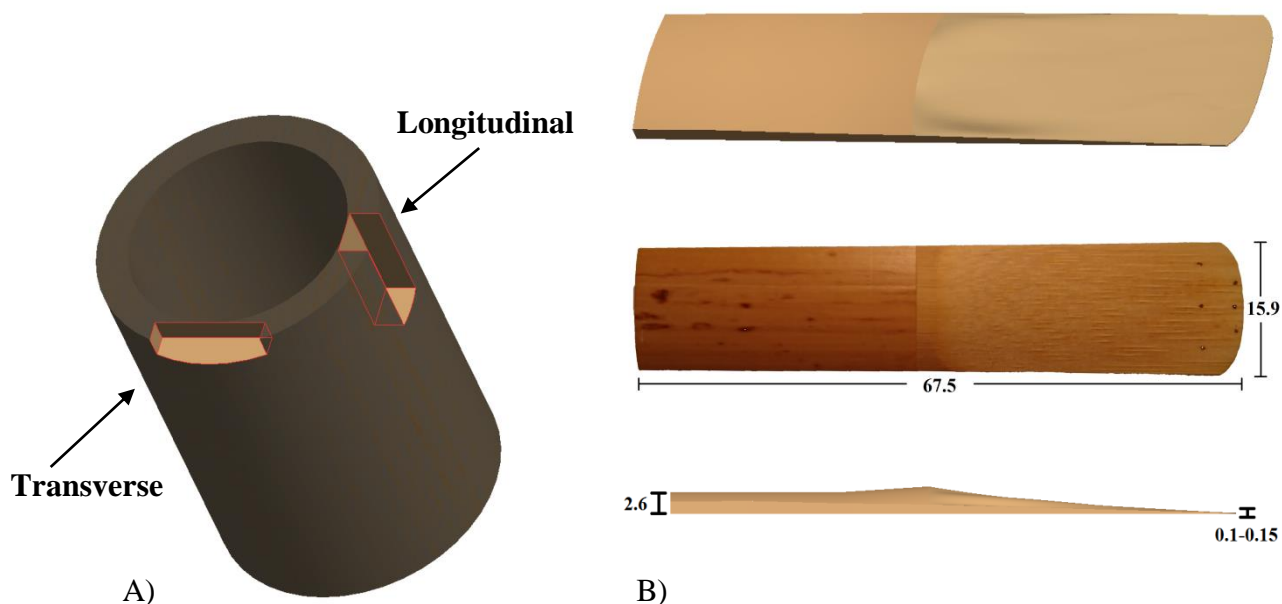


Figure 2: A) Orientation of samples used in the study with respect to the ADL stem geometry. The longitudinal sample is aligned along the length of the stem. B) Dimensions (in mm) and geometry of a typical alto saxophone reed. Note that the reed is machined from the wall of the stem and aligned with the longitudinal direction.

Each sample was a prismatic bar with equal dimensions (provided in Table 1) as this geometry lent itself well to both compression loading and bending resonance. Parallel/longitudinal samples were aligned with the fiber direction of ADL while transverse samples had a cross-section aligned with the tangential direction of the stem. The upper limit of sample thicknesses was limited by the raw ADL wall thickness. Table 1 also provides the naming convention used henceforth for the samples.

Table 1: Specimen identifiers and dimensions (in mm). Dimensions are given as a rectangular bar.

Sample	W (width)	H (height)	L (length)	Mass (g)
Longitudinal 1 (L1)	4.30	2.83	12.88	0.095
Longitudinal 2 (L2)	4.13	2.96	12.88	0.095
Transverse 1 (T1)	3.93	2.70	12.62	0.085
Transverse 2 (T2)	3.92	2.60	12.68	0.085

Cyclic mechanical loading

Samples L2 and T2 were used for the mechanical deformation component of the study. Fatigue loading was conducted on an ADMET 2.5kN material testing system using circular compression platens to prevent off-axis loading. A cycling frequency of 0.1Hz was used until 270 complete cycles had been reached. A preload was applied to each of the samples, although this load was different for sample L2 and T2 due to the added compliance of the T2 sample. This was observed from the additional strain measured for an equal load in the transverse samples, due to the loading direction being perpendicular to the fibers in the sample. Therefore, L2 was preloaded to 10 MPa and then cycled with an amplitude of ± 4.1 MPa, fully compressive. T2 was preloaded to 7 MPa and then cycled at ± 2.35 MPa. This entire iteration was completed two times, each with at least 24 hours in between to allow for residual strain to completely relax.

Residual strain is of concern due to the large relaxation times associated with viscoelastic materials such as ADL.

Moisture cycling

Samples L1 and T1 were used for the moisture cycling portion of this study. Samples were initially measured and weighed to quantify the moisture uptake during each cycle of the test. For this cycling, each sample was placed in a temperature and humidity controlled incubator at 37°C and 90% relative humidity (RH) for 24 hours. It should be noted that in-use reeds are in contact with saliva. The moisture parameters used here were taken as a first approximation of in-use conditions, where variables including pH levels, wetting preferences (i.e., not all musicians prepare reeds the same way) and embouchure (i.e., amount of the reed fully inside the mouth) were neglected. By incubating the samples at the given temperature and RH values, inter-sample variability was controlled. Given the length of incubation for each sample, moisture content was not at equilibrium. After the test, samples were then measured and weighed again before being returned to the incubator at 45°C and ambient RH to dry for 24 hours. This formed a complete cycle for the test and was repeated once. This single repeat was completed as a method of observing initial changes to the ADL material as noted by musicians upon playing a new reed for the first several sessions (where reeds are not exposed to moisture for the same length of time by all musicians).

Internal friction measurements

Measurements of internal friction were taken prior to beginning mechanical loading or moisture cycling in order to obtain an initial value for each sample. The resonant bar method [3] was used to excite each sample at frequencies between 100 and 1000 Hz (100 Hz intervals) and the resulting decay waveform was recorded upon cessation of the driving force. As these samples are extremely small with little mass, care was taken to position the specimens upon ultra-thin wire guides $0.224L$ from each end (where L is ~ 13 mm for each sample). These positions have been shown to be the nodal positions for prismatic bars of rectangular cross section in fundamental flexural vibration modes [4]. Excitation was completed using a compression driver (JBL 2426H) connected to a signal generator. Excitation tones were pure sinusoids and were applied for 2 seconds with the corresponding decay being measured for a further 1 second. Samples were positioned on the guide wires in the center of the compression driver with the specimen long-axis parallel to the driver face. This was done to ensure flexural excitation. The corresponding displacement amplitudes were measured at the center of the specimen on the opposite face using a STIL confocal white-light sensor. The entire experimental setup for these measurements is provided in Figure 3.



Figure 3: Experimental setup for internal friction measurements depicting the sample, confocal displacement sensor and compression driver.

The main advantage of this setup in comparison with the typical torsion pendulum is the complete free-free nature of sample vibration with no physical contact of any kind (i.e., no attached mass to alter the resonance of the system).

The logarithmic decrement for internal friction measurements is calculated as the relative magnitude of successive peaks in the decay amplitude plot. In order to obtain an average value over the entire decay the decrement, Δ , is calculated as follows:

$$\Delta = N^{-1} \ln \frac{A_1}{A_{N+1}} \quad (1)$$

where A_1 is the first decay peak amplitude and A_{N+1} is the $N+1$ th decay peak amplitude. An example decay curve is provided in Figure 4.

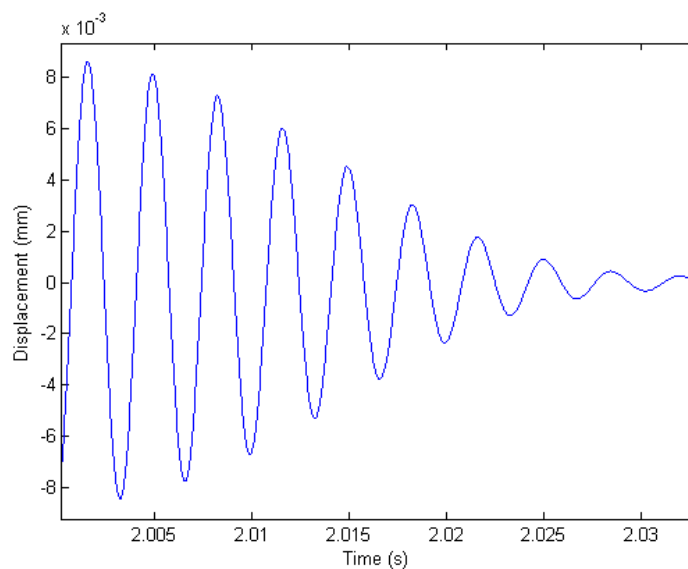


Figure 4: Sample displacement decay curve obtained at 300Hz excitation.

In total, 10 of these measurements were made per sample, per trial. To observe internal friction changes, measurements were made immediately following the first moisture cycle (samples still at 37°C and 90% RH) and 1 hour following the first 270 cycles of mechanical loading. In this way, the effects of moisture and residual strain on internal friction could be captured. These measurements were repeated one day later (24°C and ambient RH) after samples L1 and T1 had dried and samples L2 and T2 had fully relaxed. Once completed, the process was repeated again for another 24 hr/270 cycle moisture/mechanical loading.

Materials quantification

Microstructural analysis of each sample was completed through optical microscopy of cross-sections. Micrographs of samples at 5, 20, 50 and 100x were obtained in order to evaluate the distribution of microstructural features pertinent to ADL. Some of these features are illustrated in Figure 5 below.

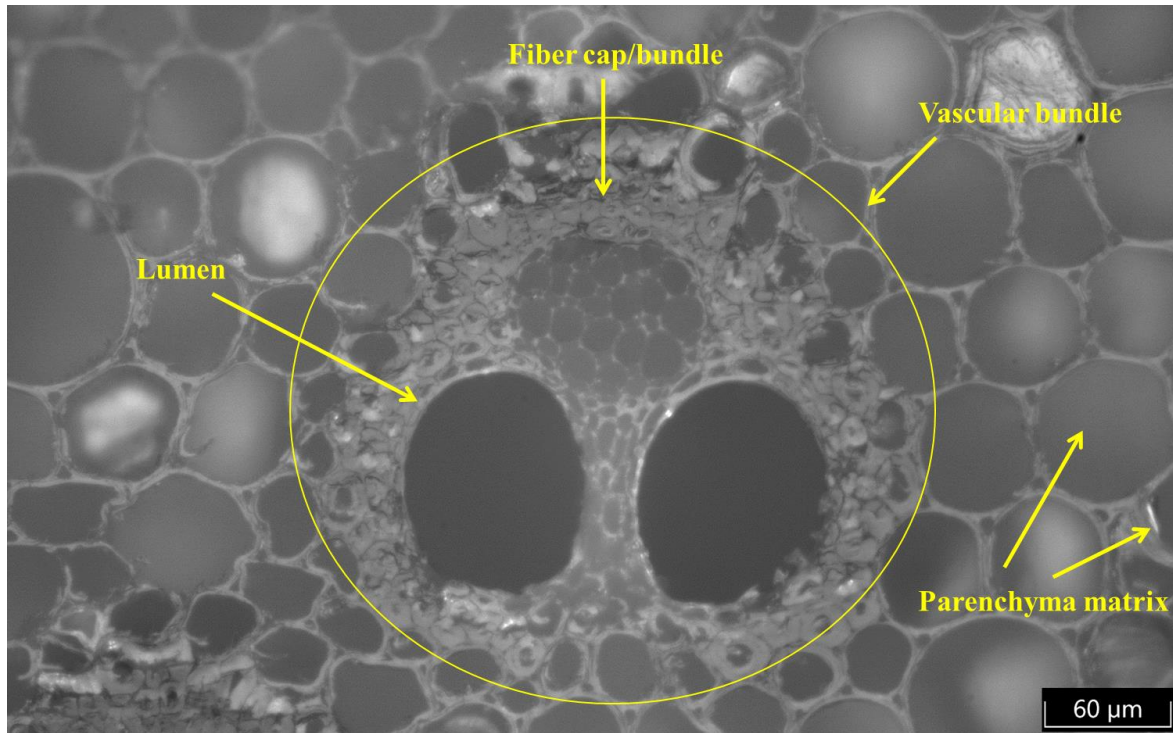


Figure 5: Optical micrograph of ADL indicating several microstructural features.

Analysis of these features over a relatively large cross-sectional area (~2 x 1 mm) provided average values for vascular bundle size, lumen diameter, parenchyma matrix diameter, fiber bundle size and vascular bundle orientation (in degrees relative to the sample surface). As an example, the vascular bundle illustrated in Figure 5 was considered to have an orientation of 0° as it is aligned with the surface.

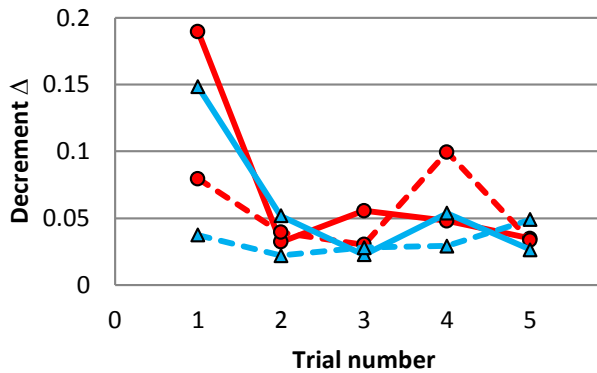
The effects of moisture on the ADL material structure was also examined through the use of XRD measurements. Measurements were made on samples L1 and T1 prior to moisture cycling, and post moisture cycling for each trial. A Bruker X8 diffractometer was used with a Cu x-ray source and 2θ values ranging from 2 to ~110°. For the case of ADL, this enabled the measure of relative phase changes between trials.

DISCUSSION

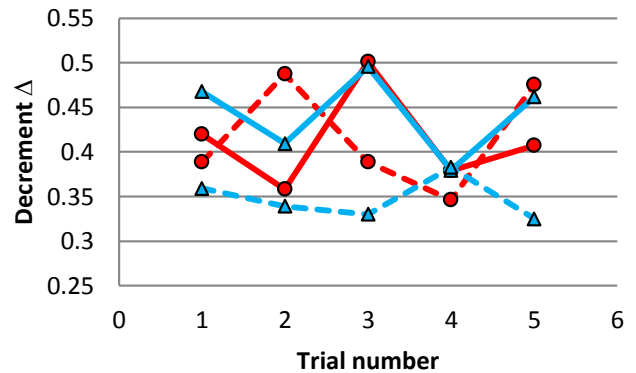
Figures 6 and 7 depict internal friction variation with frequency for all samples. Analysis of internal friction measurements shows that behavior differs between low (< 400 Hz) and high frequencies (up to 1000 Hz). As a general observation, it appears that internal friction between sample groups differs more significantly at frequencies < 400 Hz, while a general trend appears for all samples above 600 Hz. Each trial number indicates one of the 5 data points taken for logarithmic decrement values from 100 Hz to 1000 Hz (i.e., trial 1 contains 10 data points for each sample) over the course of the experiment. The timeline of the experiment is provided in Table 2, where trial 1 is the first set of measurements taken and trial 5 is the last. In the subsequent plots, the solid lines indicate samples having undergone moisture cycling, while dashed lines indicate compression loading samples.

Table 2: Experimental timeline for all ADL samples. The arrows indicate the conditioning that followed the previous trial. The type of conditioning performed on each sample is also indicated.

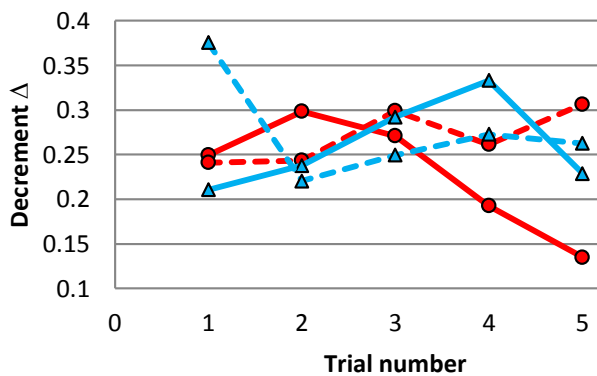
Timeline	Conditioning (Samples L1 and T1)	Conditioning (Samples L2 and T2)
	 Longitudinal 1  Transverse 1	 Longitudinal 2  Transverse 2
Trial 1 →	<i>Initial characterization</i>	
	24 hrs. at 37°C and 90% RH	Compression loading - 270 cycles
Trial 2 →	<i>Measurement 2</i>	
	24 hrs. at 45°C and ambient RH	24 hr. strain relaxation
Trial 3 →	<i>Measurement 3</i>	
	24 hrs. at 37°C and 90% RH	Compression loading - 270 cycles
Trial 4 →	<i>Measurement 4</i>	
	24 hrs. at 45°C and ambient RH	24 hr. strain relaxation
Trial 5	<i>Measurement 5</i>	



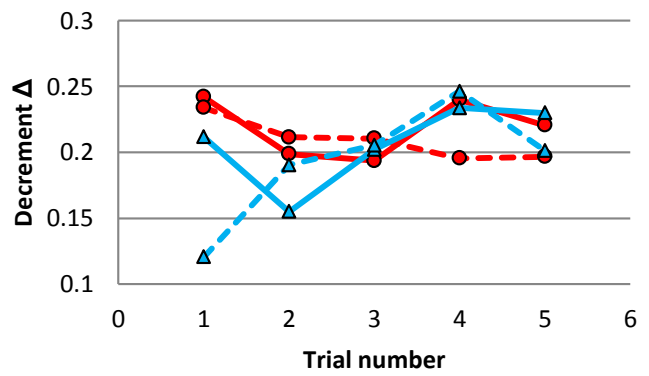
A) 100 Hz



B) 200 Hz



C) 300 Hz



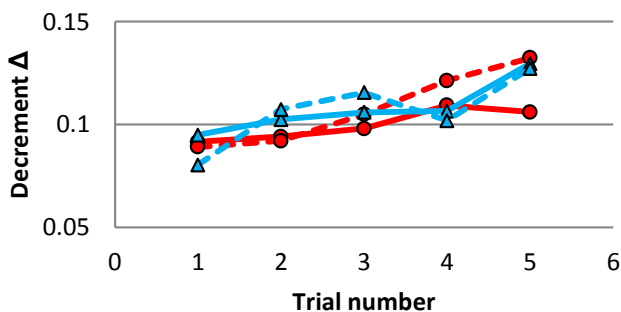
D) 400 Hz

Figure 6: Plots of internal friction given as the logarithmic decrement versus trial number for all samples. (a) 100 Hz, b) 200 Hz, c) 300 Hz, d) 400 Hz)

The low frequency internal friction results shown here do not exhibit any overall trends, however there are a few interesting sample differences. The internal friction of L2 at 100Hz seems to exhibit a dependency on strain relaxation as illustrated by the difference between trials 4 and 5.

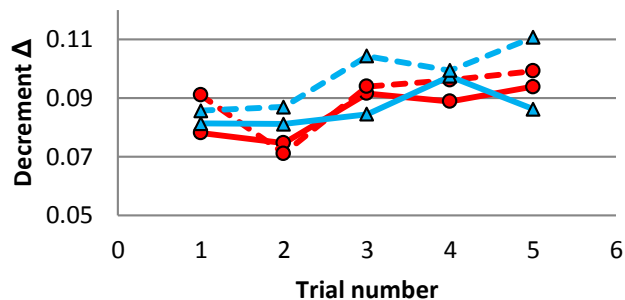
Examination of the initial versus final plots of internal friction for each sample indicates that the 100 Hz decrement value converges for all samples, suggesting that mechanical loading and moisture cycling has a similar effect on low frequency damping. Further examination indicates that this trend does not continue for the 200 Hz case. Here the largest differences (when compared to initial values) are observed for the mechanically loaded specimens (L2 and T2).

$\Delta L_{200\text{Hz}}$ increases compared to its initial value while $\Delta T_{200\text{Hz}}$ decreases by a similar amount relative to its initial value. This can be further observed by examining the plots of initial internal friction and final internal friction (after completion of all testing) in Figure 8.



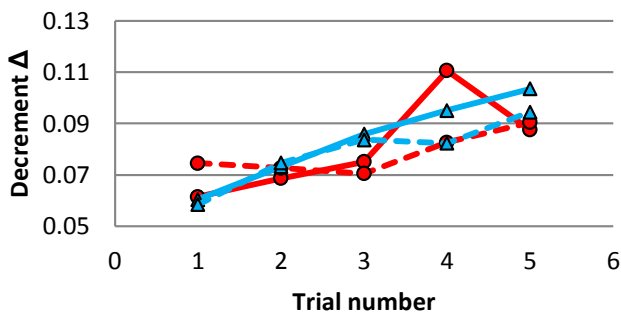
● Longitudinal 1 ● Longitudinal 2
 ▲ Transverse 1 ▲ Transverse 2

A) 700 Hz



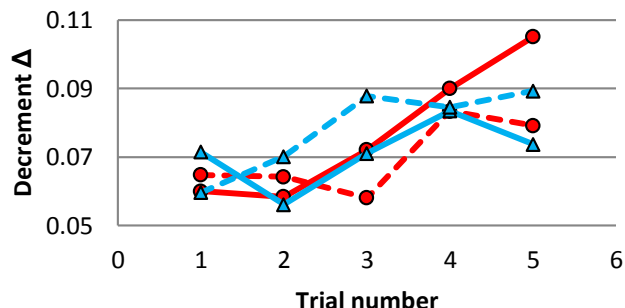
● Longitudinal 1 ● Longitudinal 2
 ▲ Transverse 1 ▲ Transverse 2

B) 800 Hz



● Longitudinal 1 ● Longitudinal 2
 ▲ Transverse 1 ▲ Transverse 2

C) 900 Hz



● Longitudinal 1 ● Longitudinal 2
 ▲ Transverse 1 ▲ Transverse 2

D) 1000 Hz

Figure 7: Plots of internal friction given as the logarithmic decrement versus trial number for all samples. (a) 700 Hz, b) 800 Hz, c) 900 Hz, d) 1000 Hz)

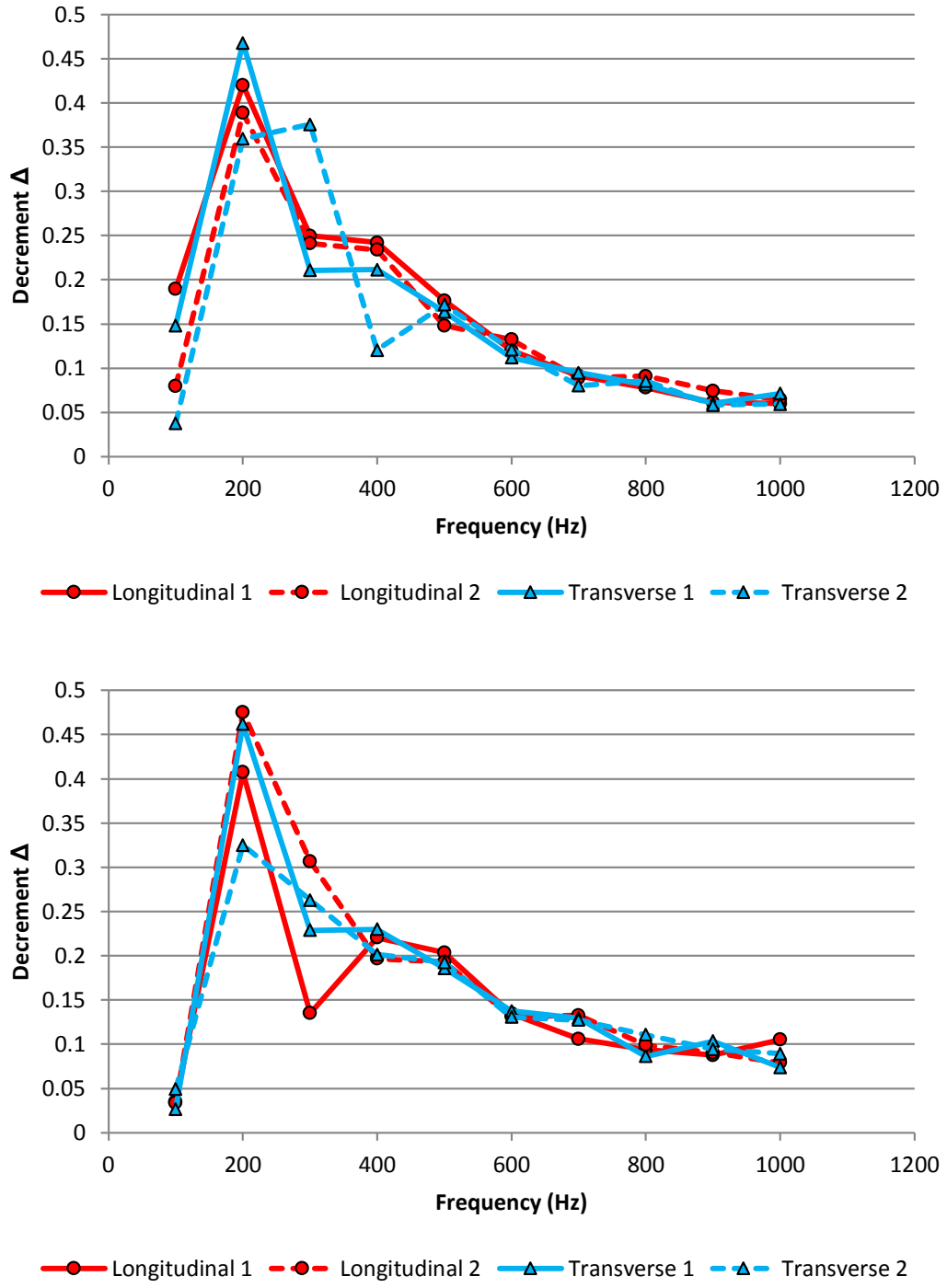


Figure 8: Top: decrement versus frequency values for all samples prior to testing. Bottom: the same results for all samples post testing.

For the case of $f = 700$ Hz, examining the trends of L1 and L2, it appears that both mechanical and moisture cycling contribute to increasing internal friction, although the rate of increase is larger for mechanical loading. Also of interest is the recovery of the 900 Hz internal friction value for L1 between the final moisture cycle measurement and the final measurement in

dry conditions. This could be indicative of the increased molecular mobility of cellulose within the fiber cap at 90% RH which adds to dissipative forces. Work on cellulose nanocomposites has suggested that increased molecular mobility (above the glass transition temperature) contributes to changes in the complex modulus of the material [5]. For moso bamboo, studies have also shown the storage modulus to be dependent on temperature and moisture (decreasing with overall moisture content and decreasing with increasing temperature) [6]. The glass transition temperature of hemicelluloses in moso bamboo has also been shown to be below 30°C, a fact which compares favorably with the assertion that increased molecular mobility is increasing internal friction for the 900Hz L1 sample at 90% RH.

Examining the results between 200 and 400 Hz more closely, it can be seen that moisture cycling has a larger effect on internal friction than mechanical loading for the case of the longitudinal samples. Specifically, at 200Hz both L1 and T1 appear to be significantly effected by moisture cycling with internal friction values decreasing with each moisture cycle. This also occurs for the 100Hz internal friction values and will be discussed in a subsequent section within the context of changing crystallinity values for L1 and T1. For the transverse samples, both mechanical loading and moisture cycling result in a large absolute change in internal friction (relative to initial values). In fact, moisture cycling appears to consistently lower the internal friction of sample L1, while cyclic mechanical loading has the opposite effect. This could be related to sample L1 having a very low average vascular bundle orientation angle indicating an increased contribution of solid fibers to recoverable, elastic energy propagation due to more homogeneous moisture expansion (this is investigated further in the microstructural analysis section).

Looking at the data for moisture uptake (24 hrs. at 90% RH) of samples L1 and T1 it is found that the maximum linear expansion is found in the width direction for L1 3.6% (corresponding to the tangential direction). For T1, a maximum linear expansion of -1.97% is found in the height direction (corresponding to the radial direction). This suggests that the material behaves very anisotropically with regards to expansion and contraction, a fact that has been mentioned in previous work on bamboo preservation [7]. It could be suggested then that the majority of residual strains due to moisture cycling would be absorbed in the parenchyma matrix due to its lower volumetric density. This data will be confirmed with longer term exposure to 90% RH.

Overall it appears that there is an internal friction peak near 200 Hz. Tests were not conducted below 100 Hz as previous results for bamboo [8] indicate that there is little internal friction dependency on frequency in this range. Although all samples appear to exhibit similar decrement values above 700 Hz, it should be noted that in terms of loss angle these small differences represent changes of 10° to 20°. Changes of this magnitude would result in a much larger viscous component of stress-strain phase lag.

Microstructural Analysis

The results of microstructural analysis are not surprising given that the four samples were machined from the same raw stem. It can be noted however that the variation in vascular bundle orientation is indicative of significant spatial variability within the single stem and may be of importance for ensuring reed tip uniformity. The results are illustrated in Figure 9.

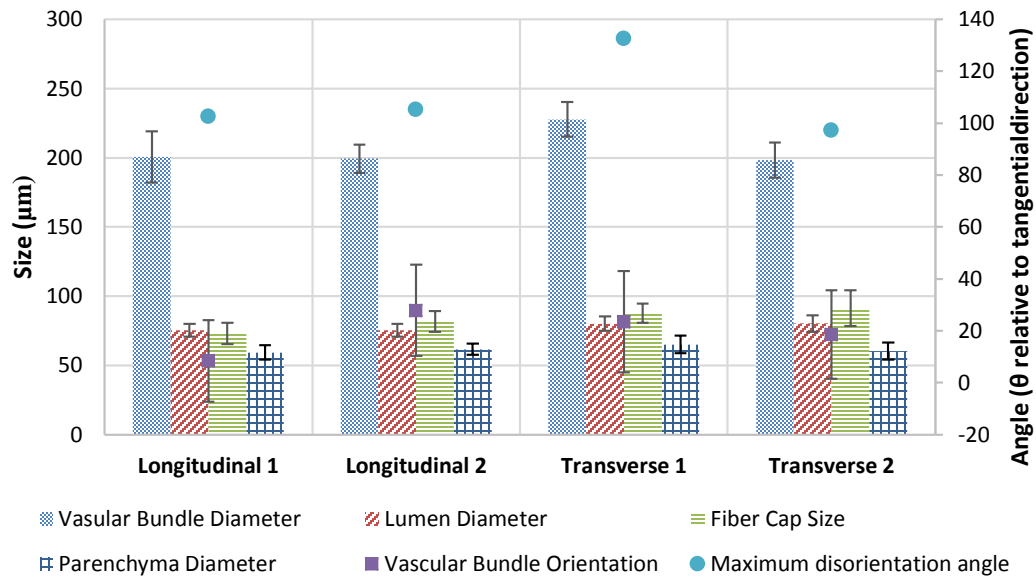


Figure 9: Microstructural results for each of the samples as measured using optical microscopy. Error bars indicate standard deviation.

The results shown in Figure 9 compare favorably with previously obtained results for reed cross-sections [9, 10]. The influence of these microstructural features on decrement values was investigated using regression analysis (with 95% confidence). For Trial 5 decrement values (the final test of each sample), a statistically significant result was obtained for vascular bundle diameter effects on internal friction at 700 Hz. Here a positive linear trend is observed where increasing vascular bundle angle (with respect to parallel alignment with the tangential direction) corresponds to increasing decrement values (F-test, $p = 0.0435$). For Trial 1 a similar observation is made for the relationship between parenchyma matrix diameter and internal friction. In this case, at 1000 Hz a positive linear trend indicates that increasing parenchyma diameter increases the logarithmic decrement (F-test, $p = 0.0259$). Increasing the size of the parenchyma cells would increase the hemicellulose and amorphous cellulose weight fractions within the sample and thus increase viscoelasticity and the effects of loss mechanisms, making this an expected result. The power of this analysis will be improved in future work by increasing the number of samples within the data set.

Inspection of the micrographs confirms the existence of cracks within the material (provided in Figure 10), both along the fiber-matrix interface and within the fiber cap. The consequences of this with regards to internal friction have been mentioned for the case of $f = 800$ Hz.

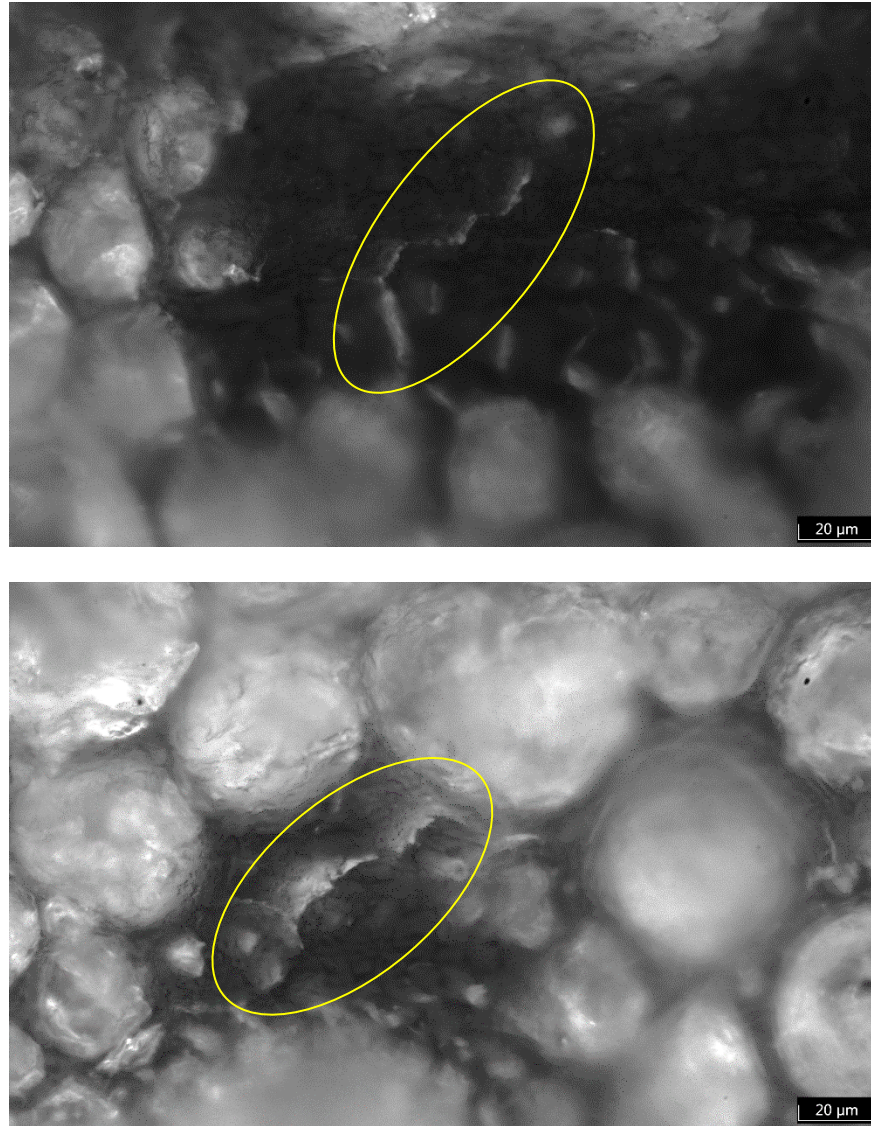


Figure 10: Micrographs of sample L1 depicting cracks within the fiber cap (top) and at the interface between the fiber cap and the parenchyma matrix (bottom).

For the case of sample L1 the nucleation of these cracks is likely the result of local differences in swelling behavior. Bamboo, a similar material to ADL, expands most significantly in the longitudinal direction [8] and for the case of sample L1 this could explain the large relative increases in internal friction above 700 Hz. These relative differences in internal friction are shown in Figure 11, where differences between Trial 1 and Trial 5 decrement values for each sample are presented as fractions of the initial value. These increases in decrement values could be attributed to the nucleation and growth of the noted cracks in between the fiber cap and matrix. This would result in a larger phase lag between these two microstructural entities for a propagating stress wave due to more viscous dissipation. While these cracks are small, the effect would contribute to high frequency internal friction values more significantly than low frequency values. This is because cracks along the fiber-matrix interface would result in large local elasticity changes (when the material is thought of as a phase weight-averaged composite) and the ratio of propagation wavelength to crack length decreases (further increasing dissipation).

Results are also given for sample L2 in Figure 12. Here large cracks within the fiber cap and significant parenchyma matrix deformation are observed. This is considered an expected result for a mechanically cycled sample.

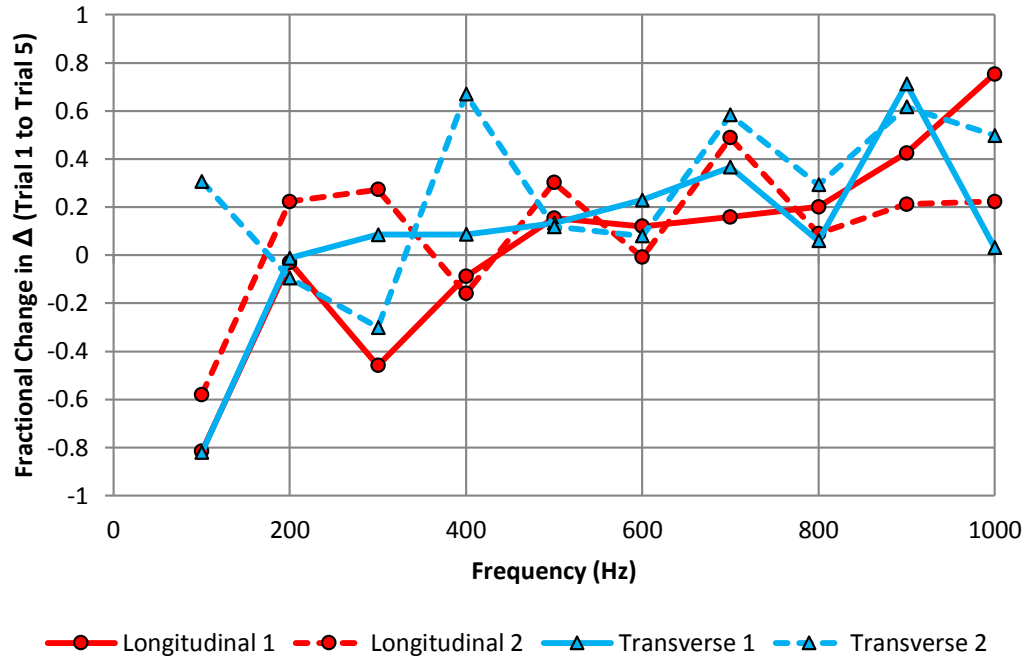
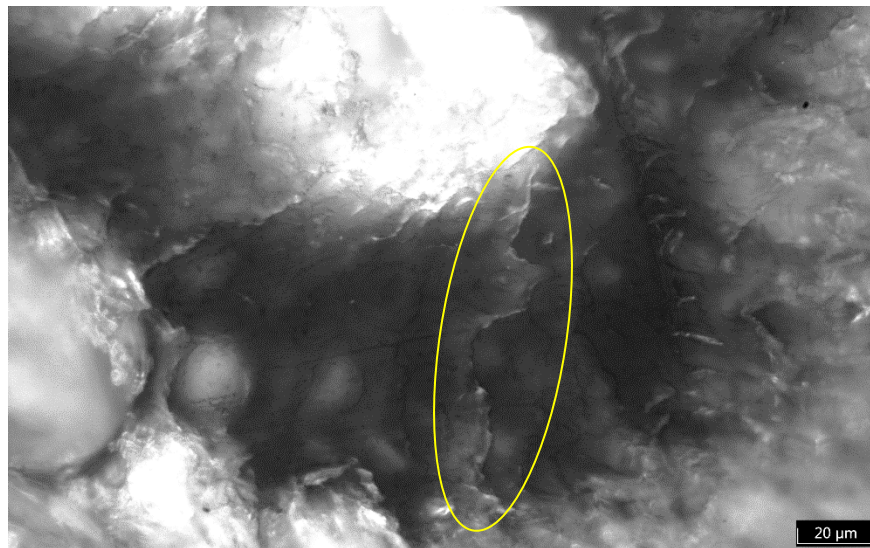


Figure 11: Change in decrement values from Trial 1 to Trial 5 for all samples. Negative values indicate a decrease in internal friction relative to the initial value, while positive values indicate an increase.



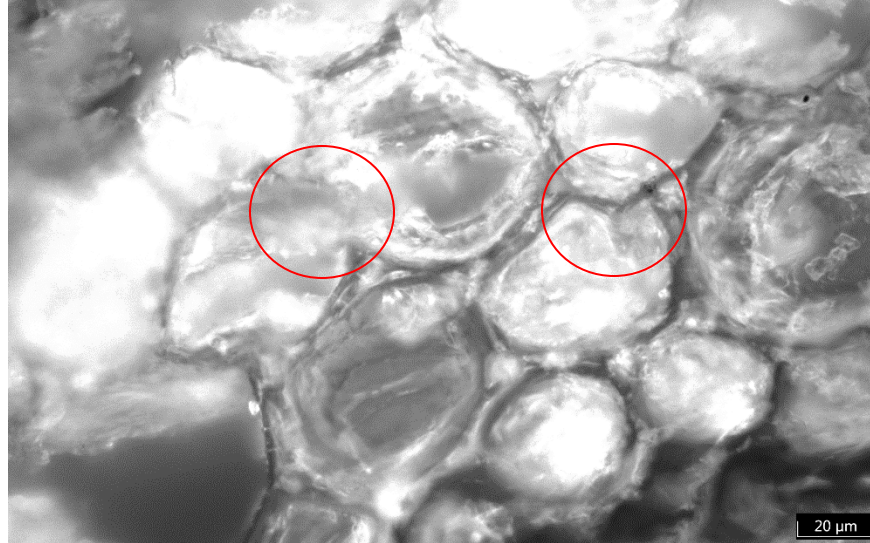


Figure 12: Micrographs of sample L2 depicting cracks within the fiber cap (top) and deformation and cell wall breakage within the parenchyma matrix (bottom).

The large increases in decrement values at 1000 Hz for the T2 sample may be explained by the complete separation of the fiber structure from the remaining vascular bundle (Figure 13). If the material is imagined as a either a Voigt (equal strain) or Reuss (equal stress) composite, the propagation of waves through the sample involves each of the phases present. In the case of T2, the resulting load sharing would be shifted mainly to the surrounding parenchyma matrix, increasing viscous dissipation as the out-of-phase response of the matrix and fiber structure increases.

Crystallinity was measured using the results of XRD measurements through the peak deconvolution method [11]. The main peak observed is for the (002) I_{β} -cellulose reflection, as shown in Figure 14. Percent crystallinity was 21.36 % for L1 and 26.06% for T1 initially. This is an expected result as the samples were cut from the same raw stem.

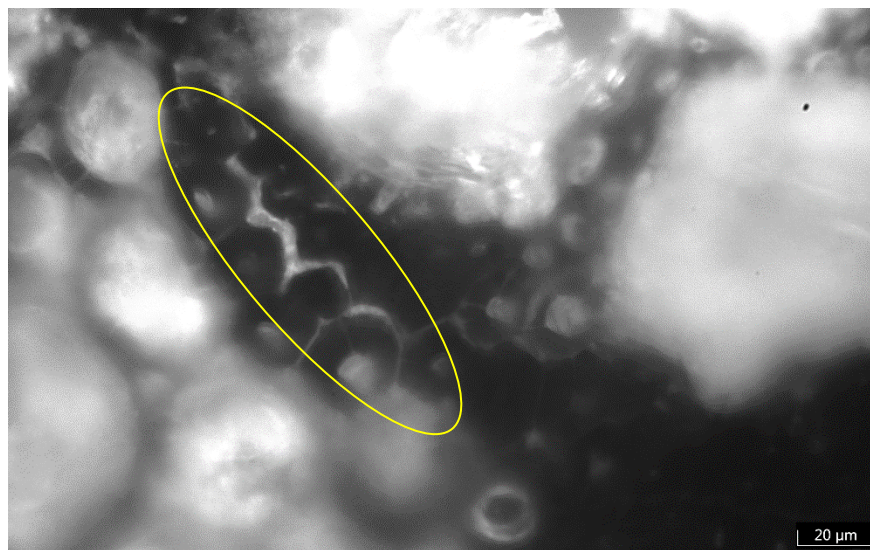


Figure 13: Complete separation of fiber cap from the vascular bundle in sample T2.

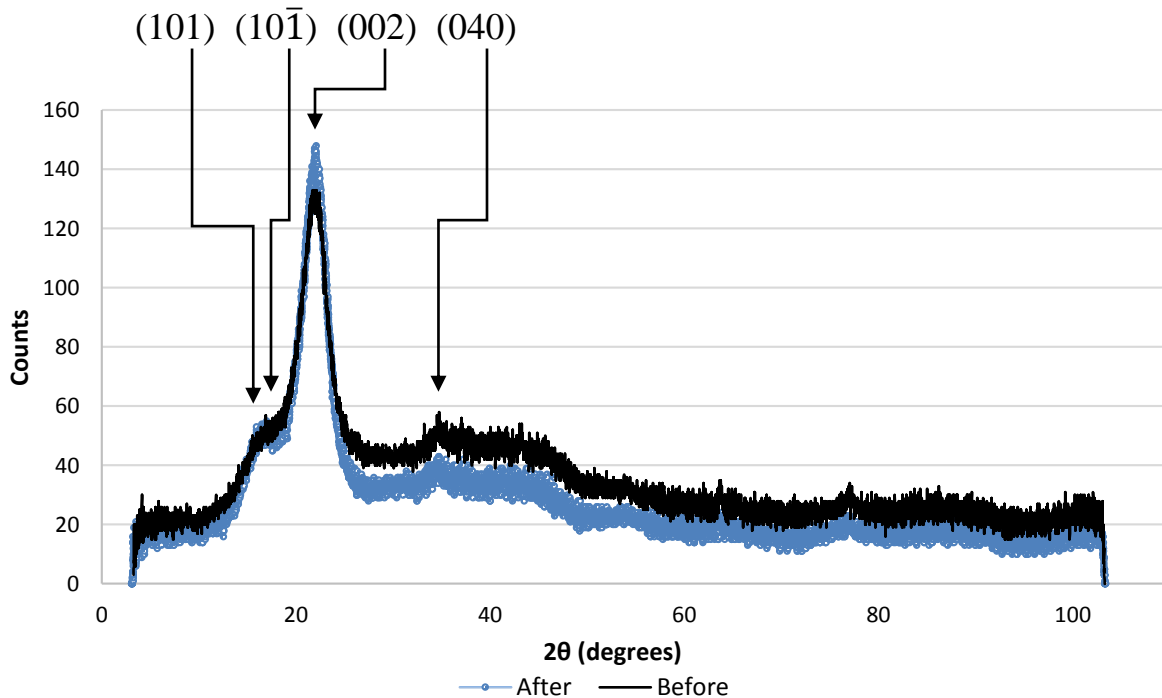


Figure 14: Before testing and after testing (both iterations) XRD spectra for sample L1. Indices of peak reflections are also provided. The lower spectrum represents the results after moisture cycling (measured after trial 5).

It is expected that normal usage of reeds (and ADL material) would contribute to changes in crystallinity due to the lower pH of saliva versus deionized water. Changes in crystallinity over time are currently being examined for real in-use reeds using the XRD technique.

Recent work on viscoelasticity in bamboo [13] indicates that at frequencies above ~ 10 Hz the viscoelastic contributions of the solid fibers and parenchyma matrix begin to equally control the dynamic behavior of the material. This manifests itself in the form of constantly increasing loss modulus (E'') values with increasing frequency. The loss modulus is related to the logarithmic decrement and represents viscous loss in the material. This could help explain the increase of internal friction (when comparing the initial to final values, as in Figure 11) observed in the present study above 700 Hz where the contributions of the parenchyma matrix and solid fibers (specifically their amorphous components) dominate the dynamic behavior. Previous research [12] on wood used in violins has indicated that specimens with larger crystalline cellulose volume fractions result in reduced loss tangent values (where the loss tangent, $\tan\delta$ is related to the logarithmic decrement by $\tan\delta = \Delta/\pi$). For this reason, ADL specimens from different stems are currently being evaluated with XRD to evaluate the importance of sample crystallinity on low frequency (< 300 Hz) internal friction.

Summary and Future Work

The preliminary work in this study has shown that internal friction of ADL (as measured by the logarithmic decrement) exhibits a sensitivity to frequencies in the range of 100 to 1000 Hz. Additionally, both mechanically loading (fatigue) and moisture cycling of samples results in changes to these measurements that are not fully recovered. The variability in sample behavior for specimens cut from a single stem internode lends credence to the musical knowledge of inter-reed variability within a package (for this case inter-stem variability has been controlled). It was also discovered that mechanically fatiguing samples and moisture cycling them contributes to internal friction results in similar ways for high frequencies (increases the logarithmic decrement) and in different ways for low frequencies (more inter-sample variation, dependent on material orientation). These two test cases are common for in-use reeds and may explain why musicians do not find reeds to behave similarly (due to different loading conditions associated with embouchure pressure).

For samples at high frequency (> 700 Hz), increasing internal friction with further trials was attributed to the development of cracks within the microstructure of each sample. For the moisture cycled samples, these cracks are a result of highly anisotropic swelling/shrinkage within the solid fiber bundles. Cracks in the mechanically loaded samples were most prevalent in the transverse sample, which was an expected result given the low E and E' moduli value in the tangential direction relative to the longitudinal direction. Analysis of microstructural features indicates subtle differences between samples, mainly vascular bundle orientation, fiber cap size and parenchyma cell diameter. At 700Hz, a statistically significant result was found via regression analysis of vascular bundle orientation versus internal friction where increasing orientation angle corresponded to increasing decrement values. At 1000Hz, a similar positive relationship between parenchyma cell diameter and internal friction was observed. Both of these results suggest that reeds comprised of high angle vascular bundles and large parenchyma cells would exhibit increased internal losses at 700 Hz and 1000 Hz.

Future work will include further analysis of XRD measurements, including estimate of cellulose crystallite size for comparison with literature values for wood and bamboo. Analysis of XRD measurements between samples will be performed and could elucidate the origins of initial internal friction variability, specifically at frequencies below 300 Hz. These results are not discussed here as further testing of a greater number of samples is required. Additionally, consideration of moisture content variation of in-use reeds (during and between playing) needs to be considered in order to validate and/or understand the limitations of using high (>90%) RH values for simulated degradation. This will also enable more long-term studies of crystallinity change with moisture cycling. Measurements of internal friction using a shaker rig will also be completed to compare free-free results with fixed-free. In this case internal friction will be measured by extracting the Lissajous curve between stress and strain ($\tan\delta$) and comparing new results with the current data. Decrement values will also be measured for longitudinal modes in addition to flexural bending (as was the case in this portion of the study). Similar results obtained for bamboo have indicated significant anisotropy in internal friction measurements [8]. Future XRD measurements will be statistically tested with internal friction values to evaluate potential correlation. Comparison with previous work on bamboo [8] will also be made by testing samples at frequencies < 100 Hz.

Measurements of loss angle will also be made through fatigue testing (0.1 Hz) of specimens with strain gauges (phase lag between stress and strain). Through a conversion of loss

angle values to logarithmic decrement values, comparison will be made with the current results. This will also facilitate comparisons of samples between stems as only intra-stem variability was observed presently. Finally, nanoindentation tests on fiber bundles and parenchyma cell walls will be completed in order to capture potential changes in reduced modulus with moisture cycling and variations through thickness of the stem wall.

ACKNOWLEDGMENTS

The authors wish to acknowledge Dr. Francois Barthelat of the Laboratory for Advanced Materials and Bioinspiration at McGill University for helpful discussions and equipment access. The same thanks are also extended to Dr. Larry Lessard of the Advanced Composite Materials Lab at McGill University for microscopy access. Discussions with Dr. Shang in the department for Materials and Mining Engineering at McGill University also helped in analyzing XRD measurements.

REFERENCES

1. P. Picart, J. Leval, F. Piquet, J. P. Boileau, T. Guimezanes, and J. P. Dalmont, *Strain*, vol. 46, no. 1, pp. 89–100, Feb. 2010.
2. E. Obataya and M. Norimoto, *J. Acoust. Soc. Am.*, vol. 106, no. 2, pp. 1106–1110, Aug. 1999.
3. I. G. Ritchie and Z.-L. Pan, *Metall. Trans. A*, vol. 22, no. 3, pp. 607–616, Mar. 1991.
4. I. G. Ritchie, *J. Sound Vibration*, vol. 31, no. 4, pp. 453–468, Dec. 1973.
5. Lars Berglund, in *Nat. Fibers, Biopolym., Biocompos.*, 1st ed., Taylor & Francis, 2005, pp. 807–817.
6. Z. Liu, Z. Jiang, Z. Cai, B. Fei, Y. Yu, and X. 'e Liu, *BioResources*, vol. 7, no. 2, pp. 1548–1557, Feb. 2012.
7. Satish Kumar, KS Shukla, Tndra Dev, and PB Dobriyal, *International Network for Bamboo and Rattan*, Oct. 1994.
8. S. Amada and R. S. Lakes, *J. Mater. Sci.*, vol. 32, no. 10, pp. 2693–2697, May 1997.
9. P. Kolesik, A. Mills, and M. Sedgley, *Ann. Bot. (Oxford, U.K.)*, vol. 81, no. 1, pp. 151–155, Jan. 1998.
10. H.-C. Spatz, H. Beismann, F. Brüchert, A. Emanns, and T. Speck, *Philos. Trans. R. Soc., B*, vol. 352, no. 1349, pp. 1–10, Jan. 1997.
11. S. Park, J. O. Baker, M. E. Himmel, P. A. Parilla, and D. K. Johnson, *Biotechnol. Biofuels*, vol. 3, p. 10, May 2010.

12. V. Bucur, in *Handbook of Materials for String Musical Instruments*, Springer International Publishing, 2016, pp. 283–323.

13. M. K. Habibi, L. Tam, D. Lau, and Y. Lu, *Mech. Mater.*, vol. 97, pp. 184–198, Jun. 2016.